Journal of Advanced Ceramics
2022, **11**(5): 794–804
https://doi.org/10.1007/s40145-022-0573-7
ISSN 2226-4108
CN 10-1154/TQ

Research Article

A high-entropy spinel ceramic oxide as the cathode for proton-conducting solid oxide fuel cells

Yangsen XU[a,†], Xi XU[b,†], Lei BI[a,*]

[a]*School of Resource Environment and Safety Engineering*, *University of South China*, *Hengyang 421001*, *China*
[b]*Department of Materials*, *Imperial College London*, *London SW72BP*, *UK*

Received: July 15, 2021; Revised: January 14, 2022; Accepted: January 16, 2022

Abstract: A high-entropy ceramic oxide is used as the cathode for the first time for proton-conducting solid oxide fuel cells (H-SOFCs). The $Fe_{0.6}Mn_{0.6}Co_{0.6}Ni_{0.6}Cr_{0.6}O_4$ (FMCNC) high-entropy spinel oxide has been successfully prepared, and the *in situ* chemical stability test demonstrates that the FMCNC material has good stability against CO_2. The first-principles calculation indicates that the high-entropy structure enhances the properties of the FMCNC material that surpasses their individual components, leading to lower O_2 adsorption energy for FMCNC than that for the individual components. The H-SOFC using the FMCNC cathode reaches an encouraging peak power density (PPD) of 1052 $mW \cdot cm^{-2}$ at 700 ℃, which is higher than those of the H-SOFCs reported recently. Additional comparison was made between the high-entropy FMCNC cathode and the traditional $Mn_{1.6}Cu_{1.4}O_4$ (MCO) spinel cathode without the high-entropy structure, revealing that the formation of the high-entropy material allows the enhanced protonation ability as well as the movement of the O p-band center closer to the Fermi level, thus improving the cathode catalytic activity. As a result, the high-entropy FMCNC has a much-decreased polarization resistance of 0.057 $\Omega \cdot cm^2$ at 700 ℃, which is half of that for the traditional MCO spinel cathode without the high-entropy design. The excellent performance of the FMCNC cell indicates that the high-entropy design makes a new life for the spinel oxide as the cathode for H-SOFCs, offering a novel and promising route for the development of high-performance materials for H-SOFCs.

Keywords: proton-conducting oxides; high-entropy oxides; cathode; solid oxide fuel cells (SOFCs)

1 Introduction

Solid oxide fuel cells (SOFCs) offer an eco-friendly and efficient way of converting chemical energies into electricity [1,2]. Due to the restriction of the traditional high-temperature SOFCs, the development of SOFCs working at intermediate temperatures is the trend, and proton-conducting SOFCs (H-SOFCs) offer a great promise in this aspect [3–5]. H-SOFCs that use protonic ceramic membrane as the electrolyte are also known as the protonic ceramic fuel cells (PCFCs). They can work at intermediate temperatures (500–700 ℃) because the proton-conducting electrolyte shows adequate conductivity at intermediate temperatures [6,7], meeting the demand of the electrolyte used for this temperature range. However, the cathode reaction becomes sluggish

† Yangsen Xu and Xi Xu contributed equally to this work.
* Corresponding author.
E-mail: lei.bi@usc.edu.cn

when the operation temperature decreases, requiring the development of new cathode materials with high performance at intermediate temperatures [8].

In the past few decades, many cathode materials have been proposed for H-SOFCs, and most cathodes are based on the perovskite or perovskite-related structures [9,10]. Some of these cathodes show good performance for H-SOFCs. Compared with the intensively investigated perovskite cathodes, spinel oxides have received less attention as the cathode for SOFCs, but they have been widely used as the coating layer for the interconnects of SOFCs [11,12]. Recently, some spinel oxides have been used as the cathode for oxygen-ion conducting SOFCs, reaching good fuel cell performance [13,14]. This result suggests that some spinel oxides could show good catalytic activity towards oxygen reduction reaction (ORR) at intermediate temperatures, thus providing an alternative option for the cathode material for SOFCs. In addition, spinel oxides are usually used as the protective coating layer for the interconnect materials in SOFCs, and the use of spinel cathodes may improve the compatibility between the cathode layer and the interconnected part. However, to the best of our knowledge, spinel oxides have not been used for H-SOFCs before. The suitability of spinel oxides as the cathode for H-SOFCs is still unknown, and it would be interesting to explore the possibility of using spinel oxide cathode for H-SOFCs. Furthermore, high-entropy ceramics were proposed a few years ago as they show unique features [15,16], and high-entropy ceramic oxides that could stabilize equimolar mixtures in the oxide have been used in many applications, achieving good performance [17–19]. Recently, the high-entropy perovskite oxide has been proposed as the cathode for traditional oxygen-ion conducting SOFCs, restricting the segregation of the Sr element at the cathode surface [20]. However, the use of the high-entropy oxides for SOFCs just begins, and the reports in this aspect are scarce, leaving many scientific issues in the structure–property relationship unclear. In addition, the high-entropy ceramic cathode has not been used as the cathode for H-SOFCs before, and the exploration of the application of high-entropy ceramic cathode in H-SOFCs is fascinating. Based on the above thinking, in this study, a high-entropy spinel oxide as a cathode for H-SOFCs is proposed, which combines both the concepts of high-entropy ceramic and spinel cathode, and aims to explore a new type of cathode for H-SOFCs with high performance. By comparing the high-entropy spinel oxide performance with a traditional spinel oxide without the high-entropy structure using both experimental studies and theoretical calculations, the mechanism for the high-entropy spinel oxide in performance enhancement is revealed.

2 Materials and method

The $Fe_{0.6}Mn_{0.6}Co_{0.6}Ni_{0.6}Cr_{0.6}O_4$ (FMCNC) high-entropy oxide was synthesized by a modified sol–gel method [21] using metal nitrates as the starting materials. The synthesized powder was calcined at 950 ℃ for 3 h to get a pure phase. The phase purity of the powder was examined by X-ray diffraction (XRD). XRD instrument (DX-2700BH, Haoyuan Instrument) was employed to perform both ordinary and *in situ* XRD tests for the FMCNC powder, in the 2θ range of 10°–85° with a scan rate of 3 (°)·min^{-1}. The tube current and voltage used in XRD were 40 mA and 40 kV, respectively. The step length of the XRD during the test was 0.02°. The chemical stability of the powder in CO_2 was examined by treating the powder at 600 ℃ in an atmosphere (10% CO_2 + 90% air) and *in situ* recording the XRD pattern of the sample. The morphology and the elements of the powder were observed using the scanning transmission electron microscope (STEM, JEM-2100F). The reference materials, including Fe_3O_4, Mn_3O_4, Co_3O_4, NiO, and Cr_2O_3, are simple metal oxides, and they are commercially available from Aladdin Industrial Corporation. The purity of all metal oxides is 99%, 99.5%, 99.9%, 99%, and 99.95% for Fe_3O_4, Mn_3O_4, Co_3O_4, NiO, and Cr_2O_3, respectively. The first-principles calculation was carried out to investigate the properties of the oxides, using the density functional theory (DFT) method [22] with the Vienna *ab initio* simulation package (VASP) [23,24]. Hubbard's correction was applied for the calculation of the transition metal elements, and the U_{eff} value was set to be 5.3, 3.9, 3.7, 6.2, and 3.32 eV for Fe, Mn, Cr, Ni, and Co, respectively. O_2 adsorption calculations were performed by simulating the O_2 adsorption procedure on the surface of the oxides. The vacuum layer with a thickness of 15 Å was constructed for the surface calculations. The calculation details can be found in our previous studies [25–27].

For the fuel cell tests, FMCNC cathode was deposited on the $BaCe_{0.7}Zr_{0.1}Y_{0.2}O_{3-\delta}$ (BCZY) half-cell that consisted of BCZY electrolyte and NiO–BCZY anode, followed by calcination in the microwave sintering

furnace at 900 ℃. In the previous study, it is found that the microwave sintering method can adhere the cathode layer to the electrolyte layer using a relatively lower sintering temperature and shorter dwell time compared with the conventional sintering method [28]. The low sintering temperature and short dwell time allow the cathode to keep the desired microstructure and mitigate the interfacial reaction, benefiting the cathode performance. The BCZY electrolyte powder was also synthesized by the modified sol–gel method. NiO–BCZY was prepared by mixing the BCZY powder with NiO powder. The half-cell fabrication procedure can be found in our previous studies [28,29]. The H-SOFC using the FMCNC cathode was tested at different temperatures using an electrochemical workstation (Squidstat Plus, Admiral Instrument). Wet H_2 was used as the fuel with a flow rate of 30 mL·min^{-1}, while static air was used at the cathode side. For comparison, the cell using the $Mn_{1.6}Cu_{1.4}O_4$ (MCO) cathode was prepared and tested under the same condition, aiming to reveal the influence of the high-entropy structure on the performance of the spinel oxide. Electrochemical impedance spectroscopy (EIS) measurements were carried out under the open circuit condition.

3 Results and discussion

Figure 1(a) shows the scheme for the preparation of the FMCNC high-entropy oxide, and the powder was synthesized by a wet chemical route to produce FMCNC nanoparticles. Figure 1(b) shows the XRD pattern of the FMCNC oxide after being fired at 950 ℃ for 3 h, confirming a pure spinel structure (PDF#79-1744) without detectable secondary phase and agreeing with the previous literature [30]. The transmission electron microscopy (TEM) image shown in Fig. 1(c) indicates that the particle size of the FMCNC is 100–150 nm. The high-resolution TEM (HRTEM) of the FMCNC shown in Fig. 1(d) indicates a *d*-spacing value of

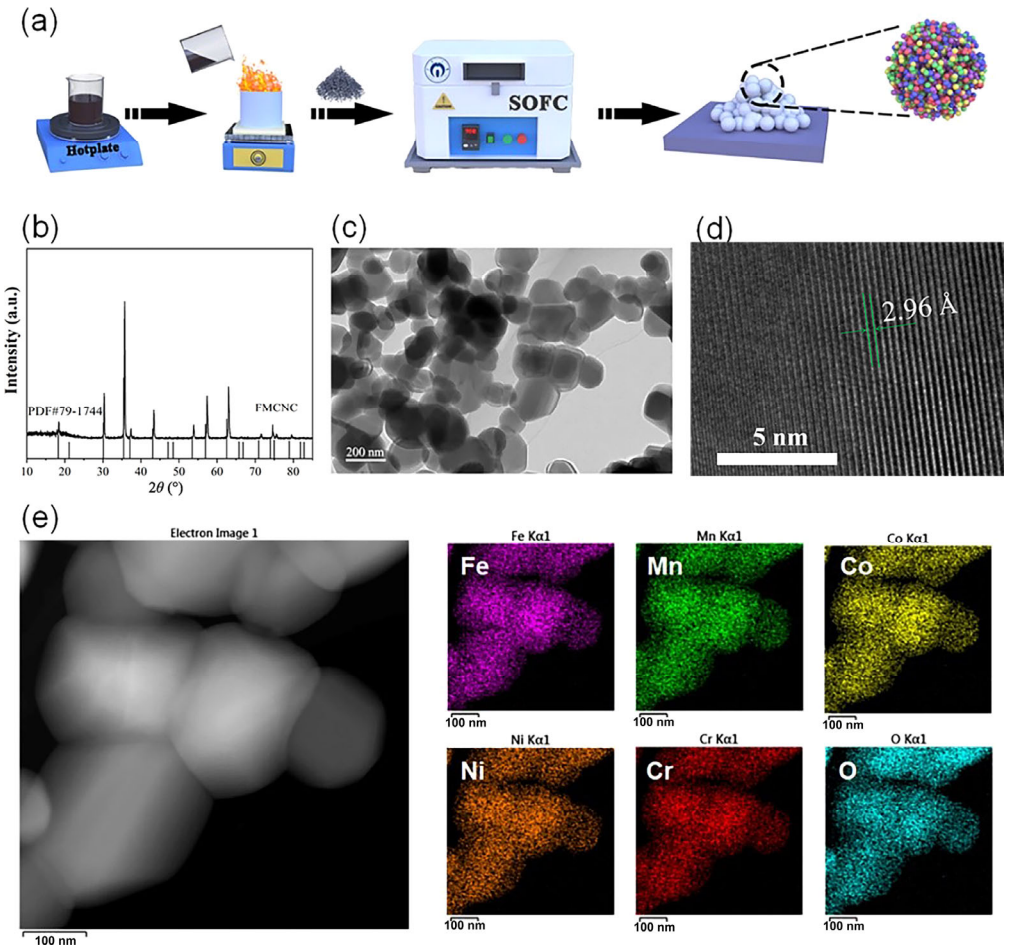

Fig. 1 (a) Scheme for the preparation of FMCNC powder; (b) XRD pattern with the reference PDF#79-1744; (c) TEM and (d) HRTEM images for the synthesized FMCNC; (e) HADDF images of the FMCNC powder with the distribution of elements.

2.96 Å, corresponding to the (220) plane of the material. Figure 1(e) shows the elemental distribution of the FMCNC characterized by STEM–high angle annular dark-field (HAADF), indicating a homogenous distribution of the Fe, Mn, Co, Ni, and Cr elements. No elemental segregation can be observed. The FMCNC material contains five different metal cations with equal content, meeting the criteria of the definition for the high-entropy ceramic that contains near-equimolar five or more principal elements [16,17]. In addition, the FMCMC shows good phase stability at high temperatures. Figure S1 in the Electronic Supplementary Material (ESM) shows the structure of the FMCNC at different temperatures recorded by high-temperature XRD (HT-XRD), and the annealing time at each temperature point is 1 h. No phase change can be detected for FMCNC from room temperature up to 900 ℃, suggesting good phase stability of FMCNC even at high temperatures.

Besides good phase stability, the FMCNC shows good chemical stability against CO_2. Figure 2 presents the time course of XRD patterns for a duration of 12 h under CO_2-containing atmosphere (10% CO_2 + 90% air) at 600 ℃. The XRD measurement was carried out every half hour. The *in situ* XRD analysis indicates that only the presence of the FMCNC phase could be detected even under the CO_2 atmosphere at a high temperature without any trace of metal carbonate or any other impurities, suggesting that there is no reaction between FMCNC and CO_2, and FMCNC has good chemical stability against CO_2. It should be noted that the CO_2 concentration in the air is about 0.03%. The concentration

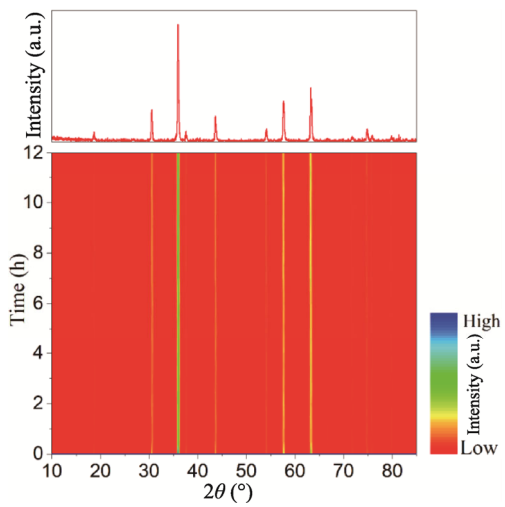

Fig. 2 *In situ* XRD measurements of FMCNC powder at 600 ℃ under CO_2-containing atmosphere as a function of time. XRD pattern of the FMCNC after 12 h exposure is on the top.

of 10% CO_2 used in this study is more than 300 times higher than that in the air, which is sufficient to demonstrate the stability of the FMCNC. Besides the stability against CO_2, its stability in the humidified condition is also important as the cathode is exposed to the produced H_2O for H-SOFCs. The stability of FMCNC under the humidified condition was examined by treating the FMCNC powder in a 30% H_2O-containing atmosphere at 600 ℃ for 10 h. XRD was used to characterize the phase of the FMCNC powder before and after the treatment. The result is shown in Fig. S2 in the ESM, indicating that there is no appearance of any new phases after the treatment, thus suggesting excellent chemical stability of FMCNC under the humidified condition.

The concept of using high-entropy ceramics is to enhance the properties of the high-entropy material that surpasses the individual components [17]. In this study, the corresponding component for FMCNC is Fe_3O_4, Mn_3O_4, Co_3O_4, NiO, and Cr_2O_3. Therefore, the comparisons between FMCNC and the other five individual components were carried out by the first-principles studies. One feature of high-entropy ceramics is the incorporation of multi-elements at a near-equimolar nature, leading to the performance enhancement with respect to the individual component, and the catalytic activity of the cathode toward O_2 is critical for the cathode performance in which the first step is the adsorption of O_2. Therefore, the ability of FMCNC for adsorbing O_2 molecular is calculated in comparison with that for Fe_3O_4, Mn_3O_4, Co_3O_4, NiO, and Cr_2O_3. The HRTEM of FMCNC suggests the *d*-spacing value for the (220) plane, indicating the exposed surface is (001) plane. Therefore, the (001) surface was used for the O_2 adsorption studies. Figure 3 shows the O_2 adsorption energy on the FMCNC surface as well as on

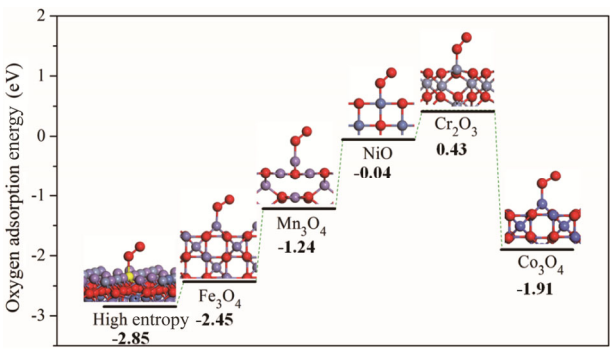

Fig. 3 Adsorption energy of O_2 on the surface of FMCNC high-entropy oxide as well as on the Fe_3O_4, Mn_3O_4, Co_3O_4, NiO, and Cr_2O_3 surfaces.

the surface of Fe_3O_4, Mn_3O_4, Co_3O_4, NiO, and Cr_2O_3 oxides. Instead of the trade-off relationship between each component, a synergy effect can be detected. The O_2 adsorption energy on FMCNC is −2.85 eV, which is obviously lower than those for Fe_3O_4, Mn_3O_4, Co_3O_4, NiO, and Cr_2O_3 oxides, suggesting the adsorption of O_2 is thermodynamically more favorable on FMCNC than that on the individual oxide. This feature could originate from the merit of the high-entropy concept, leading to an enhanced property than the individual component.

In addition to the synergy effect on the O_2 adsorption, the FMCNC high-entropy oxide shows obvious different elemental charges and oxygen vacancy contents compared with the individual oxide. Figure S3 in the ESM shows the X-ray photoelectron spectroscopy (XPS) analysis results for the transition metal elements of FMCNC, Fe_3O_4, Mn_3O_4, Co_3O_4, NiO, and Cr_2O_3 oxides. We can find the changes of the element valences in FMCNC compared with the individual oxide, suggesting the interaction among the elements. In addition, the molar ratio of adsorbed oxygen to lattice oxygen that is reported to present the content of the oxygen vacancy [31–33] increases for the FMCNC compared with that for Fe_3O_4, Mn_3O_4, Co_3O_4, NiO, and Cr_2O_3, as shown in Fig. 4 and Table 1, suggesting the FMCNC high-entropy oxide has a larger content of oxygen vacancy compared with the individual oxides. It is recognized that the oxygen vacancy content influences both the oxygen-ion migration [34,35] and the proton conduction [36,37]. Therefore, the larger oxygen vacancy content could possibly enhance the performance of the oxide for H-SOFCs.

The above studies indicate the successful preparation of the FMCNC high-entropy oxide with pure phase, and this material has good chemical stability with high prospects for H-SOFCs. Then, the FMCNC was evaluated as the cathode for H-SOFCs. It should be mentioned that the BCZY is used as the electrolyte in this study. Although FMCNC seems to react with BCZY powder after being co-fired at 900 ℃ (the cathode co-fired temperature) as shown in Fig. S4(a) in the ESM, the reaction is not evident between the FMCNC and BCZY dense electrolyte film that can be seen from Fig. S4(b) in the ESM, suggesting the reaction between BCZY dense electrolyte and FMCNC is kinetically slow, and

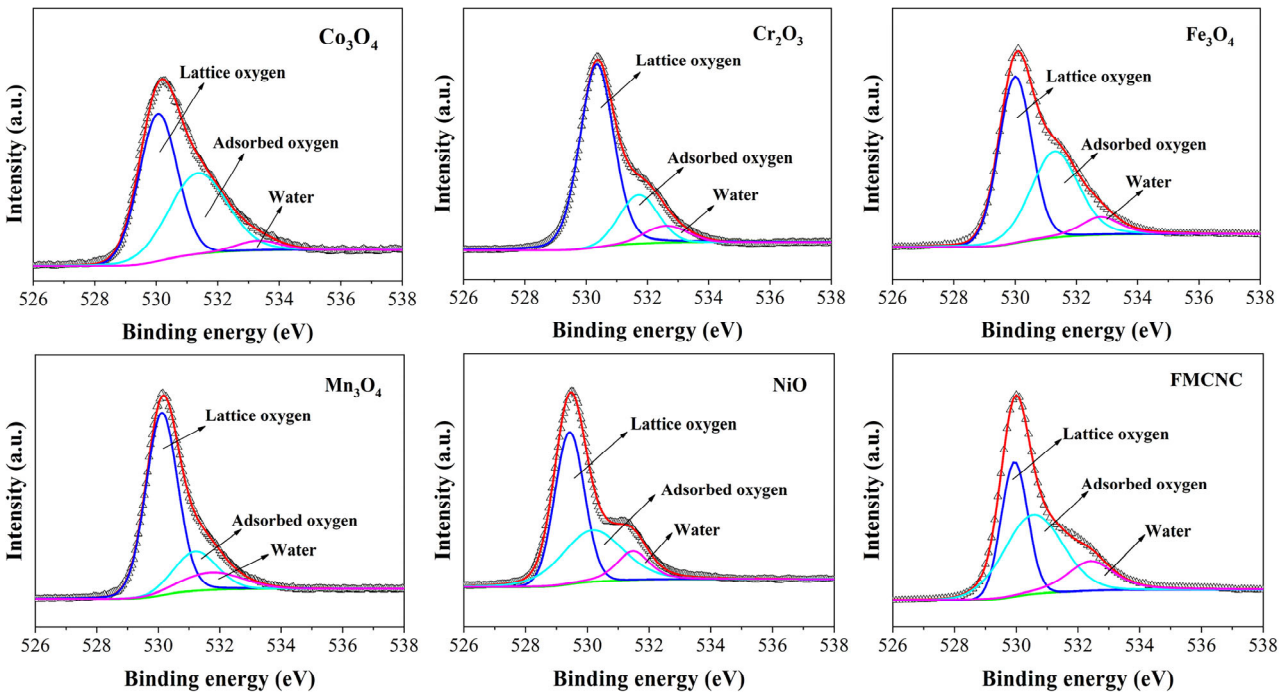

Fig. 4 XPS O 1s binding energy for FMCNC high-entropy oxide and its individual components (Fe_3O_4, Mn_3O_4, Co_3O_4, NiO, and Cr_2O_3).

Table 1 Molar ratio between adsorbed oxygen to lattice oxygen for FMCNC, Fe_3O_4, Mn_3O_4, Co_3O_4, NiO, and Cr_2O_3

	FMCNC	Fe_3O_4	Mn_3O_4	Co_3O_4	NiO	Cr_2O_3
n(adsorbed O)/*n*(lattice O)	1.33	0.78	0.77	0.85	0.75	0.68

thus avoids obvious secondary phase after being co-fired. Therefore, the FMCNC cathode material is suitable for H-SOFCs using the BCZY electrolyte. Figure 5(a) shows the cell voltage and power density vs. current density curves for the H-SOFCs using FMCNC. The peak power density (PPD) of the FMCNC cell reaches 159, 244, 453, 713, and 1052 mW·cm^{-2} at 500, 550, 600, 650, and 700 ℃, respectively. The cross-sectional views of the FMCNC cell shown in Figs. 5(b)–5(d) indicate that the cell presents a clear tri-layer structure with an electrolyte thickness of about 10 μm, and the FMCNC cathode adheres well to the electrolyte even after the fuel cell testing. It is noted that the SEM images were taken for the cell after the fuel cell testing from 700 to 500 ℃ with H_2 as the fuel and static air as the oxidant. After testing, the cell was cooled down to room temperature at a cooling rate of 5 ℃·min^{-1}. Generally, the performance of H-SOFCs is still lower than that for oxygen-ion conducting SOFCs (O-SOFCs), and the development of high-performing cathode materials is one of the most used strategies for boosting cell performance [38]. The performance of H-SOFCs has increased from tens of milliwatt per square centimetre in the early days to above 1000 mW·cm^{-2} in recent studies, mainly by using perovskite or perovskite-related cathodes [39–41]. To the best of our knowledge, spinel oxide cathodes have not been reported for the application in H-SOFCs. However, the H-SOFC using the FMCNC high-entropy oxide in the present study achieves a comparable or even higher performance compared with the reported H-SOFCs using perovskite-related cathodes [28,29], opening a new area for the design of cathodes for H-SOFCs.

To further demonstrate the influence of the high-entropy structure that promotes fuel cell performance, the FMCNC cell is compared with the H-SOFC using a typical spinel cathode oxide without the high-entropy structure. As stated above that no spinel oxide has been used as a cathode for H-SOFCs before, the high-entropy FMCNC cathode is compared with the MCO spinel cathode. MCO is selected as the reference because it has been reported to show high performance for O-SOFCs due to its good catalytic activity [14], and its performance is one of the best for SOFCs using spinel oxide cathodes. Figure 6(a) shows the comparison of the fuel cell output of the cells using the FMCNC cathode and the MCO cathode tested at 700 ℃. We can find that the cell using the MCO cathode exhibits a PPD of 593 mW·cm^{-2}. In contrast, the FMCNC cathode cell exhibits a PPD of 1052 mW·cm^{-2} under the same testing conditions. The comparison of the EIS plots for both cells measured at 700 ℃ is shown in Fig. 6(b).

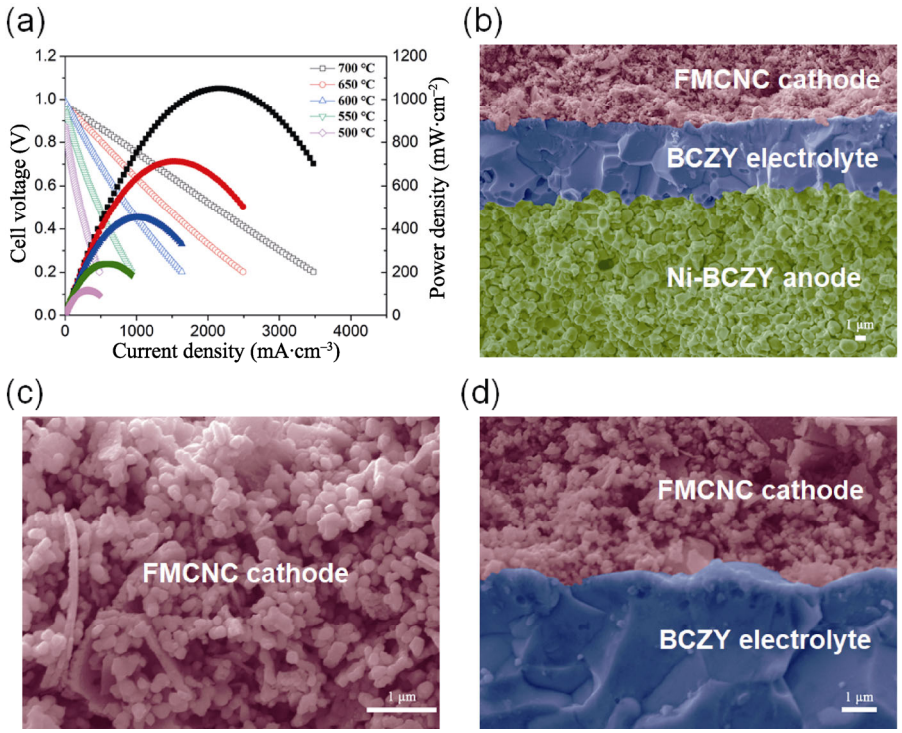

Fig. 5 (a) Cell voltage and power density vs. current density curves for FMCNC cell; SEM images of (b) FMCNC cell, (c) cathode, and (d) cathode–electrolyte interface.

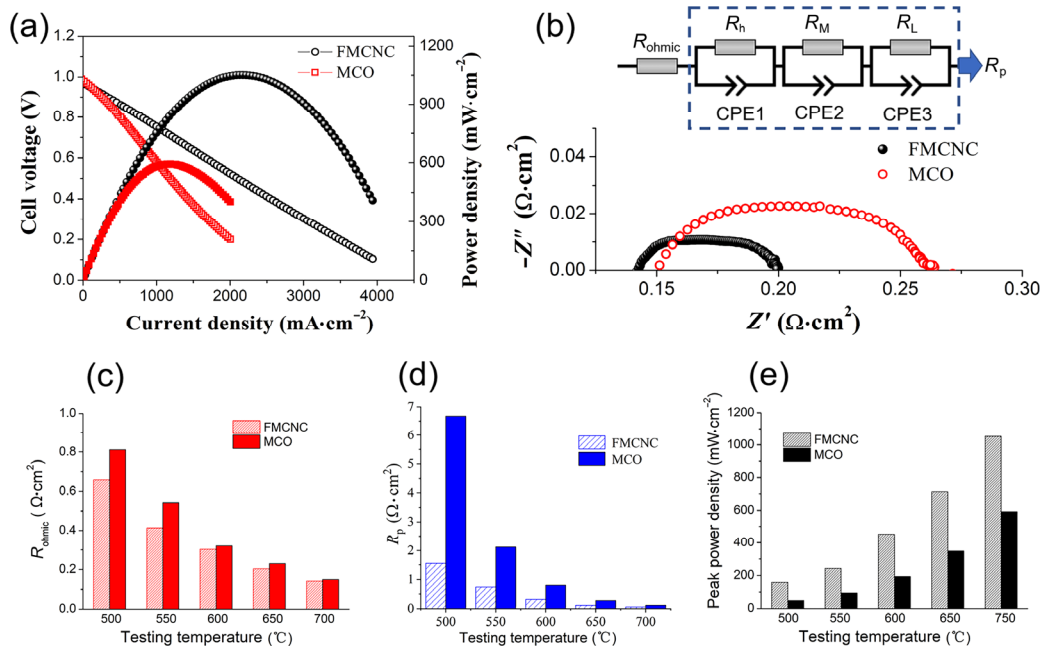

Fig. 6 Comparison of (a) fuel cell performance and (b) EIS plot for the cell using FMCNC and MCO cathodes measured at 700 ℃, and the equivalent circuit used to fit the EIS plot is inserted; comparison of the values for (c) R_{ohmic}, (d) R_p, and (e) PPD of the cell using FMCNC and MCO cathodes tested at different temperatures.

The high-frequency intercept is the ohmic resistance (R_{ohmic}), and the difference between the high-frequency intercept and low-frequency intercept is the polarization resistance (R_p). Both cells have a similar R_{ohmic} that reaches 0.15 and 0.14 Ω·cm^2 for MCO cell and FMCNC cell, respectively. In contrast, the R_p of these two cells shows a noticeable difference, being 0.118 and 0.057 Ω·cm^2 for MCO cell and FMCNC cell, respectively. The EIS plots can be fitted with the equivalent circuit. The R_{ohmic} is fitted with one resistance element, whereas the curve between the high-frequency intercept and low-frequency intercept that presents R_p can be fitted with three depressed semi-circles. Therefore, three distributed elements composed of a constant phase element (CPE) in parallel with a resistance are used to fit the R_p [42]. The R_h, R_m, and R_l mean the resistance at the high-frequency, middle-frequency, and low-frequency for the R_p arc, respectively. CPE1, CPE2, and CPE3 are the CPEs that correspond to R_h, R_m, and R_l, respectively. The R_p is the sum of R_h, R_m, and R_l. The trend for the R_{ohmic} and R_p is also observed at other testing temperatures. Figures 6(c)–6(e) show the R_{ohmic}, R_p, and the PPD for both MCO and FMCNC cells. As the temperature decreases, the conductivity of the electrolyte reduces, and the electrode reaction becomes sluggish [43,44], which leads to an increase in R_{ohmic} and R_p for both cells. We could see that the R_{ohmic} is close for both cells at different testing temperatures. The similar R_{ohmic} that mainly consists of the resistance from the electrolyte and the interfacial contacts is expected because the half cells prepared in an identical way were used. In contrast, a noticeable difference in R_p can be observed for both MCO and FMCNC cells, and the increase in R_p value is more profound for the MCO cell compared with the FMCNC cell when the testing temperature decreases. As both cells use the same anode and electrolyte, the dramatic difference in R_p mainly comes from the cathode used. The much-reduced R_p indicates that FMCNC has an improved catalytic activity than that of MCO. From the perspective of cell structure, the cell consisted of three layers, including the Ni–BCZY anode, BCZY electrolyte, and FMCNC (or MCO) cathode. The structure of the Ni–BCZY/BCZY half cells is the same for both cells, and the cathode–electrolyte interfacial structure is similar for both FMCNC and MCO cells, making R_{ohmic} similar for both cells. In contrast, the R_p comes from the reactions at the anode and cathode. The same structure of the anode leads to similar anode reaction kinetics for both cells. Therefore, the smaller R_p suggests the better catalytic activity of FMCNC, reducing the R_p values. We can also see from Figs. 6(d) and 6(e) that the cell performance is associated with the cell resistance, and the better cathode catalytic activity of FMCNC compared

with MCO is the origin for the higher fuel cell performance, suggesting the benefits of the high-entropy structure oxide for H-SOFCs.

To further explore the influence of the high-entropy structure on the key parameters in the spinel oxide for H-SOFCs, the DFT calculation was used to study the protonation ability of the material. It is widely accepted that the protonation ability is critical for the performance of cathodes for H-SOFCs. Protonic defects are formed in the oxide lattice according to Reaction (1):

$$H_2O + V_o^{\bullet\bullet} + O_o^{\times} \Leftrightarrow 2OH^{\bullet} \quad (1)$$

Therefore, the hydration formation energies (E_{hydra}) for these two spinel oxides with and without the high-entropy structure are calculated. The energies for the hydrated sample (E_{2OH}), the bulk of one defective oxygen atom (E_{defect}), and the water molecule (E_{H_2O}) were calculated with the DFT method. The E_{hydra} can be obtained with Eq. (2):

$$E_{hydra} = E_{2OH} - E_{defect} - E_{H_2O} \quad (2)$$

According to the first-principles calculation, the E_{hydra} is −0.10 and −2.85 eV for MCO cell and FMCNC, respectively. The high-entropy FMCNC spinel oxide has a significantly lower E_{hydra} than that for the traditional spinel oxide MCO, suggesting the formation of proton defects is more favorable in FMCNC than that in MCO, which is critical for the cathode reaction for H-SOFCs. Additionally, the construction of the high-entropy structure allows a closer O p-band center to the Fermi level compared with the oxide without the high-entropy structure, benefiting the ORR of the cathode. It has been identified that the O p-band center is an effective descriptor for the ORR ability of SOFC cathodes [45]. The closer of the O p-band center to the Fermi level, the easier the removal and addition of O atoms that are critical aspects for ORR are. Figure 7 shows the projected density of states (p-DOS) of the O atom for FMCNC and MCO. It can be found that the O p-band center is −2.12 and −2.56 eV for FMCNC and MCO, respectively. The O p-band center in the FMCNC high-entropy ceramic oxide is closer to the Fermi level than the spinel oxide without the high-entropy structure, suggesting that the movement of O atoms in FMCNC is more straightforward, thus helping the ORR. The above evidence indicates that the enhanced protonation ability and improved ORR ability should be the reason for the decreased R_p for FMCNC when used in H-SOFCs.

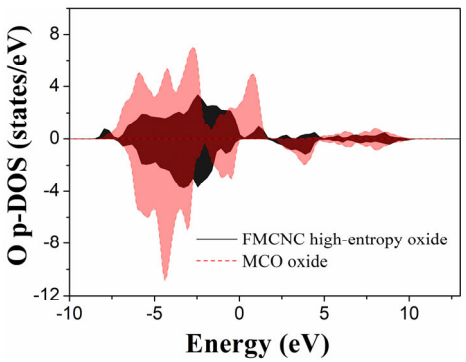

Fig. 7 O p-DOS for FMCNC high-entropy oxide and MCO oxide.

It should be noted that by coupling the spinel oxide with a high-entropy structure, the cell performance is boosted, reaching the high level for H-SOFCs, as indicated in Table 2 [40,44,46–55]. In addition to the large fuel cell output, the R_p value of 0.057 Ω·cm^2 for the FMCNC cathode is also one of the smallest values reported for H-SOFCs, suggesting that the spinel oxides could show sufficient competence as the cathodes for H-SOFCs when they are coupled with the high-entropy design. Besides the high fuel cell performance, the H-SOFC using FMCNC cathode also demonstrates good stability under the fuel cell operating condition. Figure 8 shows the result of the long-term stability test for the FMCNC cell, indicating good stability for the H-SOFC using FMCNC as the cathode. The voltage even increases a little with the increased working time. This

Table 2 Comparison of PPD and the corresponding R_p for the H-SOFC using FMCNC cathode with those recently reported in the literature. Testing temperatures are indicated

Year (Ref.)	Cathode composition	PPD (mW·cm^{-2})	R_p (Ω·cm^2)
2015 [39]	$BaCo_{0.4}Fe_{0.4}Zr_{0.1}Y_{0.1}O_{3-\delta}$	650 (at 600 ℃)	0.07
2016 [46]	$Sm_{0.5}Sr_{0.5}CoO_3$	700 (at 700 ℃)	0.1
2017 [47]	$BaCe_{0.5}Fe_{0.3}Bi_{0.2}O_3$	736 (at 700 ℃)	0.098
2017 [48]	$YFe_{0.5}Co_{0.5}O_3$	260 (at 700 ℃)	0.2
2018 [49]	$PrBa_{0.5}Sr_{0.5}Co_{1.5}Fe_{0.5}O_{5+\delta}$	800 (at 600 ℃)	0.15
2019 [50]	La_2NiO_4	508 (at 700 ℃)	0.15
2019 [50]	$LaNi_{0.6}Fe_{0.4}O_3$	551 (at 700 ℃)	0.128
2019 [51]	$Ba_{0.5}Sr_{0.5}Co_{0.8}Fe_{0.2}O_3$	960 (at 700 ℃)	0.075
2019 [52]	$La_{0.35}Pr_{0.15}Sr_{0.5}FeO_3$	1083 (at 700 ℃)	0.063
2020 [40]	$Pr_2BaNiMnO_7$	1070 (at 700 ℃)	0.084
2020 [44]	$Nd(Ba_{0.4}Sr_{0.4}Ca_{0.2})Co_{1.6}Fe_{0.4}O_5$	776 (at 700 ℃)	0.114
2020 [53]	$Ba_{0.95}Ca_{0.05}Co_{0.4}Fe_{0.4}Zr_{0.1}Y_{0.1}O_3$	580 (at 700 ℃)	0.12
2020 [54]	$Pr_{0.5}Sr_{0.5}FeO_3$	570 (at 700 ℃)	0.1
2020 [55]	$Sr_2Fe_{1.5}Mo_{0.4}Zr_{0.1}O_6$	790 (at 700 ℃)	0.169
This study	FMCNC	1052 (at 700 ℃)	0.057

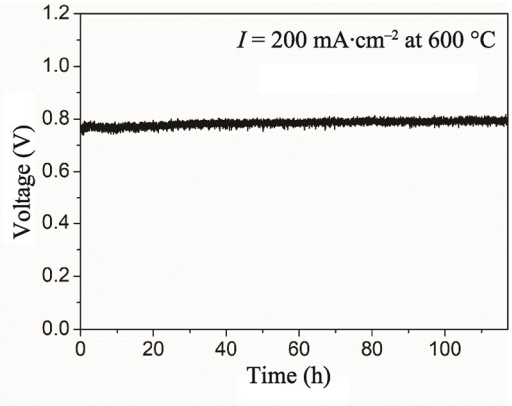

Fig. 8 Long-term stability of the FMCNC cell tested at 600 ℃.

phenomenon is probably due to the electrode activation process that is associated with the improvement in the electrode catalyst function, and has been reported in other studies for H-SOFCs [56–58]. The SEM image for the cell (Fig. S5 in the ESM) after the long-term stability test indicates that a good contact between the cathode layer and the electrolyte is still maintained, which is probably due to the excellent thermal match between the FMCNC cathode and the BCZY electrolyte. The thermal expansion coefficient (TEC) testing result for FMCNC shown in Fig. S6 in the ESM indicates that the TEC value for FMCNC is about 10.2×10^{-6} K^{-1}, which is very close to the TEC of the proton-conducting electrolyte BCZY used in this study that is reported to be about 10.1×10^{-6} K^{-1} [59]. The high-entropy FMCNC not only offers a new and compatible cathode material for H-SOFCs, but also provides a promising strategy of designing spinel cathodes.

4 Conclusions

In the present study, the concept of high-entropy ceramics is coupled with the spinel oxides, aiming to provide a novel material and a new way of designing the cathode for H-SOFCs. Although spinel oxides and high-entropy ceramics have rarely been used for H-SOFCs, the proposed FMCNC high-entropy spinel oxide has shown impressive performance as a cathode for H-SOFCs. The performance of the FMCNC cathode is improved compared with the traditional spinel oxide and comparable or even better than that of the perovskite-related cathodes that have received the most attention in the past decades. The atomic-level studies by the first-principles method indicate that FMCNC combines the merits of the individual oxides, and thus possesses a better catalytic activity towards O_2, benefiting the cathode performance. Compared with the traditional spinel oxide, the high-entropy structure of FMCNC lowers the energy for hydration and also has a closer O p-band center to the Fermi level, suggesting that the high-entropy oxide offers an improved feature of protonation and ORR activity for the H-SOFC cathode, thus clarifying the mechanism of the high-performing FMCNC that incorporates the high-entropy structure into spinel oxides for H-SOFCs.

Acknowledgements

This work is supported by the National Natural Science Foundation of China (Grant No. 51972183) and Hundred Youth Talents Program of Hunan and the Startup Funding for Talents at University of South China.

Electronic Supplementary Material

Supplementary material is available in the online version of this article at https://doi.org/10.1007/s40145-022-0573-7.

References

[1] Shin JF, Xu W, Zanella M, *et al*. Self-assembled dynamic perovskite composite cathodes for intermediate temperature solid oxide fuel cells. *Nat Energy* 2017, **2**: 16214.

[2] Su HR, Hu YH. Progress in low-temperature solid oxide fuel cells with hydrocarbon fuels. *Chem Eng J* 2020, **402**: 126235.

[3] Chen M, Xie XB, Guo JH, *et al*. Space charge layer effect at the platinum anode/$BaZr_{0.9}Y_{0.1}O_{3-\delta}$ electrolyte interface in proton ceramic fuel cells. *J Mater Chem A* 2020, **8**: 12566–12575.

[4] Zhang W, Hu YH. Progress in proton-conducting oxides as electrolytes for low-temperature solid oxide fuel cells: From materials to devices. *Energy Sci Eng* 2021, **9**: 984–1011.

[5] Wu S, Xu X, Li XM, *et al*. High-performance proton-conducting solid oxide fuel cells using the first-generation Sr-doped $LaMnO_3$ cathode tailored with Zn ions. *Sci China Mater* 2022, **65**: 675–682.

[6] Chen M, Chen DC, Wang K, *et al*. Densification and electrical conducting behavior of $BaZr_{0.9}Y_{0.1}O_{3-\delta}$ proton conducting ceramics with NiO additive. *J Alloys Compd* 2019, **781**: 857–865.

[7] Li J, Wang C, Wang XF, *et al*. Sintering aids for proton-conducting oxides—A double-edged sword? A mini review. *Electrochem Commun* 2020, **112**: 106672.

[8] Li PZ, Yang W, Tian CJ, *et al*. Electrochemical performance

of $La_2NiO_{4+\delta}$–$Ce_{0.55}La_{0.45}O_{2-\delta}$ as a promising bifunctional oxygen electrode for reversible solid oxide cells. *J Adv Ceram* 2021, **10**: 328–337.

[9] Zhou C, Sunarso J, Song YF, *et al*. New reduced-temperature ceramic fuel cells with dual-ion conducting electrolyte and triple-conducting double perovskite cathode. *J Mater Chem A* 2019, **7**: 13265–13274.

[10] Song YF, Chen YB, Wang W, *et al*. Self-assembled triple-conducting nanocomposite as a superior protonic ceramic fuel cell cathode. *Joule* 2019, **3**: 2842–2853.

[11] Sun ZH, Gopalan S, Pal UB, *et al*. $Cu_{1.3}Mn_{1.7}O_4$ spinel coatings deposited by electrophoretic deposition on Crofer 22 APU substrates for solid oxide fuel cell applications. *Surf Coat Technol* 2017, **323**: 49–57.

[12] Talic B, Molin S, Wiik K, *et al*. Comparison of iron and copper doped manganese cobalt spinel oxides as protective coatings for solid oxide fuel cell interconnects. *J Power Sources* 2017, **372**: 145–156.

[13] Liu HY, Zhu XF, Cheng MJ, *et al*. Novel $Mn_{1.5}Co_{1.5}O_4$ spinel cathodes for intermediate temperature solid oxidefuel cells. *Chem Commun* 2011, **47**: 2378–2380.

[14] Zhen SY, Sun W, Li PQ, *et al*. High performance cobalt-free $Cu_{1.4}Mn_{1.6}O_4$ spinel oxide as an intermediate temperature solid oxide fuel cell cathode. *J Power Sources* 2016, **315**: 140–144.

[15] Sun YN, Xiang HM, Dai FZ, *et al*. Preparation and properties of CMAS resistant bixbyite structured high-entropy oxides RE_2O_3 (RE = Sm, Eu, Er, Lu, Y, and Yb): Promising environmental barrier coating materials for Al_2O_3f/Al_2O_3 composites. *J Adv Ceram* 2021, **10**: 596–613.

[16] Oses C, Toher C, Curtarolo S. High-entropy ceramics. *Nat Rev Mater* 2020, **5**: 295–309.

[17] Xiang HM, Xing Y, Dai FZ, *et al*. High-entropy ceramics: Present status, challenges, and a look forward. *J Adv Ceram* 2021, **10**: 385–441.

[18] Qin MD, Yan QZ, Liu Y, *et al*. A new class of high-entropy M_3B_4 borides. *J Adv Ceram* 2021, **10**: 166–172.

[19] Zhang Y, Sun SK, Guo WM, *et al*. Optimal preparation of high-entropy boride-silicon carbide ceramics. *J Adv Ceram* 2021, **10**: 173–180.

[20] Yang Y, Bao H, Ni H, *et al*. A novel facile strategy to suppress Sr segregation for high-entropy stabilized $La_{0.8}Sr_{0.2}MnO_{3-\delta}$ cathode. *J Power Sources* 2021, **482**: 228959.

[21] Bi L, Shafi SP, Da'as EH, *et al*. Tailoring the cathode–electrolyte interface with nanoparticles for boosting the solid oxide fuel cell performance of chemically stable proton-conducting electrolytes. *Small* 2018, **14**: e1801231.

[22] Hohenberg P, Kohn W. Inhomogeneous electron gas. *Phys Rev* 1964, **136**: B864–B871.

[23] Blöchl PE, Jepsen O, Andersen OK. Improved tetrahedron method for Brillouin-zone integrations. *Phys Rev B* 1994, **49**: 16223–16233.

[24] Kresse G, Furthmüller J. Efficient iterative schemes for *ab initio* total-energy calculations using a plane-wave basis set. *Phys Rev B Condens Matter* 1996, **54**: 11169–11186.

[25] Xu X, Wang HQ, Fronzi M, *et al*. Tailoring cations in a perovskite cathode for proton-conducting solid oxide fuel cells with high performance. *J Mater Chem A* 2019, **7**: 20624–20632.

[26] Yin YR, Yu SF, Dai HL, *et al*. Triggering interfacial activity of the traditional $La_{0.5}Sr_{0.5}MnO_3$ cathode with Co-doping for proton-conducting solid oxide fuel cells. *J Mater Chem A* 2022, **10**: 1726–1734.

[27] Ji QQ, Xu X, Liu XH, *et al*. Improvement of the catalytic properties of porous lanthanum manganite for the oxygen reduction reaction by partial substitution of strontium for lanthanum. *Electrochem Commun* 2021, **124**: 106964.

[28] Wang B, Bi L, Zhao XS. Fabrication of one-step co-fired proton-conducting solid oxide fuel cells with the assistance of microwave sintering. *J Eur Ceram Soc* 2018, **38**: 5620–5624.

[29] Xu X, Bi L, Zhao XS. Highly-conductive proton-conducting electrolyte membranes with a low sintering temperature for solid oxide fuel cells. *J Membr Sci* 2018, **558**: 17–25.

[30] Grzesik Z, Smoła G, Miszczak M, *et al*. Defect structure and transport properties of $(Co,Cr,Fe,Mn,Ni)_3O_4$ spinel-structured high entropy oxide. *J Eur Ceram Soc* 2020, **40**: 835–839.

[31] Zhang XH, Pei CL, Chang X, *et al*. FeO_6 octahedral distortion activates lattice oxygen in perovskite ferrite for methane partial oxidation coupled with CO_2 splitting. *J Am Chem Soc* 2020, **142**: 11540–11549.

[32] Zhang LL, Yin YR, Xu YS, *et al*. Tailoring $Sr_2Fe_{1.5}Mo_{0.5}O_{6-\delta}$ with Sc as a new single-phase cathode for proton-conducting solid oxide fuel cells. *Sci China Mater* 2022, https://doi.org/10.1007/s40843-021-1935-5.

[33] Xu YS, Liu XH, Cao N, *et al*. Defect engineering for electrocatalytic nitrogen reduction reaction at ambient conditions. *Sustain Mater Technol* 2021, **27**: e00229.

[34] Kilner JA, Burriel M. Materials for intermediate-temperature solid-oxide fuel cells. *Annu Rev Mater Res* 2014, **44**: 365–393.

[35] Lu XK, Yang X, Jia LC, *et al*. First principles study on the oxygen reduction reaction of the $La_{1-x}Sr_xMnO_{3-\delta}$ coated $Ba_{1-x}Sr_xCo_{1-y}Fe_yO_{3-\delta}$ cathode for solid oxide fuel cells. *Int J Hydrog Energy* 2019, **44**: 16359–16367.

[36] Tao ZR, Xu X, Bi L. Density functional theory calculations for cathode materials of proton-conducting solid oxide fuel cells: A mini-review. *Electrochem Commun* 2021, **129**: 107072.

[37] Xu X, Xu YS, Ma JM, *et al*. Tailoring electronic structure of perovskite cathode for proton-conducting solid oxide fuel cells with high performance. *J Power Sources* 2021, **489**: 229486.

[38] Duan CC, Huang J, Sullivan N, *et al*. Proton-conducting oxides for energy conversion and storage. *Appl Phys Rev* 2020, **7**: 011314.

[39] Duan CC, Tong JH, Shang M, *et al*. Readily processed protonic ceramic fuel cells with high performance at low

temperatures. *Science* 2015, **349**: 1321–1326.

[40] Wang Q, Hou J, Fan Y, *et al*. $Pr_2BaNiMnO_{7-\delta}$ double-layered Ruddlesden–Popper perovskite oxides as efficient cathode electrocatalysts for low temperature proton conducting solid oxide fuel cells. *J Mater Chem A* 2020, **8**: 7704–7712.

[41] Xie Y, Shi N, Huan DM, *et al*. A stable and efficient cathode for fluorine-containing proton-conducting solid oxide fuel cells. *ChemSusChem* 2018, **11**: 3423–3430.

[42] Fabbri E, Bi L, Pergolesi D, *et al*. High-performance composite cathodes with tailored mixed conductivity for intermediate temperature solid oxide fuel cells using proton conducting electrolytes. *Energy Environ Sci* 2011, **4**: 4984–4993.

[43] Tarutin AP, Lyagaeva JG, Medvedev DA, *et al*. Recent advances in layered $Ln_2NiO_{4+\delta}$ nickelates: Fundamentals and prospects of their applications in protonic ceramic fuel and electrolysis cells. *J Mater Chem A* 2021, **9**: 154–195.

[44] Chen JY, Li J, Jia LC, *et al*. A novel layered perovskite $Nd(Ba_{0.4}Sr_{0.4}Ca_{0.2})Co_{1.6}Fe_{0.4}O_{5+\delta}$ as cathode for proton-conducting solid oxide fuel cells. *J Power Sources* 2019, **428**: 13–19.

[45] Lee YL, Kleis J, Rossmeisl J, *et al*. Prediction of solid oxide fuel cell cathode activity with first-principles descriptors. *Energy Environ Sci* 2011, **4**: 3966–3970.

[46] Zhao L, Li G, Chen KF, *et al*. $Sm_{0.5}Sr_{0.5}CoO_{3-\delta}$ infiltrated $Ce_{0.9}Gd_{0.1}O_{2-\delta}$ composite cathodes for high performance protonic ceramic fuel cells. *J Power Sources* 2016, **333**: 24–29.

[47] Shan D, Gong Z, Wu YS, *et al*. A novel $BaCe_{0.5}Fe_{0.3}Bi_{0.2}O_{3-\delta}$ perovskite-type cathode for proton-conducting solid oxide fuel cells. *Ceram Int* 2017, **43**: 3660–3663.

[48] Cui JJ, Wang JK, Fan WW, *et al*. Porous $YFe_{0.5}Co_{0.5}O_3$ thin sheets as cathode for intermediate-temperature solid oxide fuel cells. *Int J Hydrog Energy* 2017, **42**: 20164–20175.

[49] Choi S, Kucharczyk CJ, Liang YG, *et al*. Exceptional power density and stability at intermediate temperatures in protonic ceramic fuel cells. *Nat Energy* 2018, **3**: 202–210.

[50] Tang HD, Jin ZZ, Wu YS, *et al*. Cobalt-free nanofiber cathodes for proton conducting solid oxide fuel cells. *Electrochem Commun* 2019, **100**: 108–112.

[51] Liu WY, Kou HN, Wang XF, *et al*. Improving the performance of the $Ba_{0.5}Sr_{0.5}Co_{0.8}Fe_{0.2}O_{3-\delta}$ cathode for proton-conducting SOFCs by microwave sintering. *Ceram Int* 2019, **45**: 20994–20998.

[52] Xu X, Wang HQ, Ma JM, *et al*. Impressive performance of proton-conducting solid oxide fuel cells using a first-generation cathode with tailored cations. *J Mater Chem A* 2019, **7**: 18792–18798.

[53] Li J, Hou J, Lu Y, *et al*. Ca-containing $Ba_{0.95}Ca_{0.05}Co_{0.4}Fe_{0.4}Zr_{0.1}Y_{0.1}O_{3-\delta}$ cathode with high CO_2- poisoning tolerance for proton-conducting solid oxide fuel cells. *J Power Sources* 2020, **453**: 227909.

[54] Ma JM, Tao ZT, Kou HN, *et al*. Evaluating the effect of Pr-doping on the performance of strontium-doped lanthanum ferrite cathodes for protonic SOFCs. *Ceram Int* 2020, **46**: 4000–4005.

[55] Ren RZ, Wang ZH, Meng XG, *et al*. Tailoring the oxygen vacancy to achieve fast intrinsic proton transport in a perovskite cathode for protonic ceramic fuel cells. *ACS Appl Energy Mater* 2020, **3**: 4914–4922.

[56] Kim J, Sengodan S, Kwon G, *et al*. Triple-conducting layered perovskites as cathode materials for proton-conducting solid oxide fuel cells. *ChemSusChem* 2014, **7**: 2811–2815.

[57] Chen Y, Yoo S, Pei K, *et al*. An *in situ* formed, dual-phase cathode with a highly active catalyst coating for protonic ceramic fuel cells. *Adv Funct Mater* 2018, **28**: 1704907.

[58] He F, Gao QN, Liu ZQ, *et al*. A new Pd doped proton conducting perovskite oxide with multiple functionalities for efficient and stable power generation from ammonia at reduced temperatures. *Adv Energy Mater* 2021, **11**: 2003916.

[59] Zhu ZW, Qian J, Wang ZT, *et al*. High-performance anode-supported solid oxide fuel cells based on nickel-based cathode and $Ba(Zr_{0.1}Ce_{0.7}Y_{0.2})O_{3-\delta}$ electrolyte. *J Alloys Compd* 2013, **581**: 832–835.